Title: Auditory Gamma-Frequency Entrainment Abolishes Working Memory Deficits in a Rodent Model of Autism

Authors: Jorge Cardoso[1,2], Marta Luis[2], Catarina Mesquita[2], Luísa V. Lopes[1,2] and Miguel Remondes[1,2,3] *

Affiliations:

[1] Gulbenkian Institute for Molecular Medicine
Lisbon, 1649-028, Portugal

[2] Faculdade de Medicina
Universidade de Lisboa
Lisbon, 1649-028, Portugal

[3] Faculdade de Medicina Veterinária
Universidade Lusófona
Lisbon, 1749-024, Portugal

***Correspondence and Lead Contact email:** miguel.remondes@gimm.pt

Summary

Individuals on the autism spectrum often exhibit atypical responses to sensory stimuli and difficulties with behavioral regulation, reflecting altered functional patterns in core sensory-motor circuits. These sensory processing differences suggest the potential for using patterned auditory stimulation to modulate neural activity and mitigate symptoms. While impairments in higher cognitive functions are a hallmark of autism, they remain underexplored in rodent models compared to basic sensory-motor deficits. In this study, we investigated higher cognitive function in the valproic acid (VPA) rodent model of autism and evaluated whether auditory entrainment could ameliorate associated impairments. Pregnant dams received an intraperitoneal injection of VPA on embryonic day 12.5 (E12.5), and offspring were subsequently tested on a delayed non-match to place (DNMP) task to assess working memory. Following 40Hz sensory entrainment,

VPA-exposed animals showed significantly impaired performance and altered trial-by-trial learning dynamics, indicating deficits in working memory-based decision making. More importantly, auditory stimulation led to increased gamma-frequency oscillations and enhanced power in other bands (theta, beta) across brain regions, as assessed by LFP recordings in freely moving animals. These neural effects were sustained even after stimulation ended, indicating robust and lasting modulation of brain dynamics.
This provides strong evidence for the therapeutic potential of sensory entrainment in reversing autism-related cognitive deficits.

Introduction

A critical component of adaptive behavior is the ability to make decisions based on the spatial structure of one's environment - a capacity broadly referred to as spatial cognition or spatial goal-directed behavior (GDB). This cognitive function begins with the selection of relevant sensory inputs from a continuous stream of stimuli and culminates in the storage of spatial representations within cortico-hippocampal circuits, forming cognitive maps characterized by diverse neural activity patterns sensitive to both egocentric (self-referenced) and allocentric (world-referenced) spatial variables [1–3].
Emerging evidence suggests that the neural circuits connecting early sensory processing, memory formation, and anterior executive regions involved in behavioral control are altered in autism spectrum disorder (ASD). These alterations may contribute to the hallmark inflexibility observed in ASD—manifesting as rigid, self-centered rather than adaptive, context-sensitive behaviors, thoughts, and emotions [4]. While a wide range of spontaneous and stimulus-driven behaviors have been documented in animals prenatally exposed to valproic acid (VPA)—a well-established rodent model of ASD—higher cognitive functions, such as spatial GDB, remain relatively unexplored in this model. If VPA exposure indeed mirrors core ASD phenotypes, deficits in early cognitive functions, including the ability to utilize allocentric spatial information to guide behavior, would be expected. Recent studies in neurodegenerative models have shown that patterned sensory stimulations - specifically sensory entrainment - can mitigate cognitive deficits [5]. Given the reliance of higher cognitive processes on effective sensory integration, we hypothesize that similar strategies may also alleviate cognitive impairments associated

with ASD. In particular, we propose that auditory gamma-frequency entrainment could enhance spatial working memory and goal-directed decision making in VPA-exposed rodents.

To test these hypotheses, we employed a Delayed Non-Match to Place (DNMP) task designed to robustly engage working memory (WM) over a 20-second delay. In subsequent sessions, animals performed this task while exposed to auditory gamma-frequency (40 Hz) entrainment. The DNMP paradigm requires animals to recall a prior spatial decision, and the time it was made, in order to disambiguate it from similar, previously rewarded decisions [6–11]. In our established version of this task [12,13], animals navigate one arm of a T-maze during a "Sample" run, followed by a 20-second delay period. In the ensuing "Test" run, both arms are made available, and a reward is given for choosing the arm opposite to the one previously sampled. We applied this paradigm to animals prenatally exposed to either saline or valproic acid (VPA; 400 or 600 mg/kg body weight, intraperitoneally administered to pregnant dams), modeling varying degrees of ASD-like traits. Importantly, animals were assigned to groups without prior behavioral screening, ensuring an unbiased approach to testing VPA's impact on memory-guided decision making.

To evaluate behavioral performance, we measured both trial-level accuracy (correct/error) and session-level success (% correct trials), analyzing outcomes across individuals, sessions, and groups (CTRL, VPA400, VPA600). To examine the impact of VPA exposure on task performance, we used a multivariable Generalized Linear Mixed Model (GLMM), accounting for both categorical and continuous predictors. Additionally, we conducted trial-by-trial analyses using logistic regression and state-space modeling to assess learning dynamics and estimate the probability of correct choices over time.

Given that perseverative behavior—a hallmark of ASD—is often maladaptive in tasks requiring cognitive flexibility, we also quantified individual perseveration biases. A bias index was computed for each animal by calculating the difference in left versus right arm choices during Test trials, normalized by the total number of trials.

To determine whether auditory entrainment could modulate the underlying neural dynamics associated with these behaviors, we recorded multi-unit neural activity using a multi-tetrode drive implanted in brain areas implicated in ASD pathogenesis. In a

dedicated experimental group (VPA600), animals underwent three consecutive blocks of six DNMP sessions, with gamma-frequency auditory stimulation applied during the middle block. Behavioral changes across these phases were assessed using the performance metrics described above, enabling us to evaluate both behavioral and neural effects of sensory entrainment.

Results

Group-level performance reveals working memory impairment following prenatal VPA exposure

In the DNMP task, animals first complete a "Sample" trial, during which one arm of the T-maze is blocked. In the subsequent "Test" trial, both arms are accessible, and rats are rewarded for choosing the arm opposite to the one previously visited during the Sample trial (Figure 1A).

A group-level analysis of performance across all animals (Figure 1B) revealed a general improvement over sessions 1 to 6 ($\chi^2 = 30.39$, $p < 0.001$; Fixed Effect Omnibus test). However, animals exposed in utero to valproic acid (both VP600 and VP400) displayed significantly impaired performance compared to control animals (CTRL), with a robust effect of treatment (Figure 1B–C; Table 2; GLMM: $\chi^2 = 15.05$, $p < 0.001$; Fixed Effect Omnibus test). No significant performance difference was observed between the VP600 and VP400 groups ($p < 0.001$, Bonferroni post hoc test). Interestingly, this performance gap disappeared by session 6, with all groups achieving accuracy well above chance (50%). Notably, the CTRL group showed a slight decline in performance by session 6.

These findings suggest that prenatal VPA exposure impairs spatial working memory (SWM) in the DNMP task. To better understand the underlying learning dynamics, we next analyzed performance progression within sessions (S1–S6) and across individual trials.

VPA-exposed animals exhibit disrupted trial-by-trial learning dynamics and reduced within-session performance stability.

To assess within-session behavioral dynamics in individual animals, we analyzed how trial-by-trial performance evolved over time. Specifically, we aimed to estimate the probability of a correct choice on each trial based on preceding trials. For this, we

employed two complementary approaches: Binary Logistic Regression (BLR) and State-Space Modeling (SSM), allowing us to track trial-wise learning and performance maintenance across sessions S1–S6 (see Supplementary Figure 1 for raw data, BLR, and SSM outputs for each animal across groups).

In CTRL animals, we observed not only a clear improvement across sessions, as shown earlier, but also a consistent within-session increase in the probability of correct responses. Both BLR and SSM analyses converged on these results, with later sessions showing high and stable performance. Group-level analyses further confirmed this pattern: in 3.2 out of 6 sessions, the 95% confidence intervals (CIs) of the mean trial-wise correct probability exceeded the 50% chance level, indicating reliable and above-chance performance (Figure 2A). On average, SSM yielded stable trial-by-trial estimates in 4.8 of 6 sessions per animal (Figure S1; Table 1).

In contrast, the VP400 group displayed markedly weaker performance. Mean correct trial probabilities were lower, and within-session learning curves were flatter or absent. Only 2.1 out of 6 sessions showed group-level 95% CIs above chance (Figure 2B), and SSM failed to provide stable performance estimates in 2.3 of 6 sessions per animal, on average, reflecting unreliable learning (Figure S1 – data for individual animals; Table 1 – group level analysis and SSM reliability).

The VP600 group, with the largest sample size, showed slightly narrower confidence intervals but significantly lower performance overall. Incremental within-session learning was infrequent, and even in later sessions (S5–S6), group-level performance remained well below CTRL levels (Figure 2C). Only 1.38 of 6 sessions, on average, yielded group-level 95% CIs above chance performance, and SSM produced stable trial-wise estimates in just 3.2 of 6 sessions per animal (Figure S1 – data for individual animals; Figure S2 – Logit and SSM data, with 95% CIs for each individual animal, Table 1 – group level analysis and SSM reliability).

Together, these findings indicate that while VPA-exposed animals are eventually able to reach a performance plateau, their overall success is significantly diminished compared to controls. More importantly, analysis of trial-by-trial dynamics reveals that past trials in VPA animals are poor predictors of future behavior. This inconsistency prevents reliable estimation of learning progression, as only a minority of sessions show performance

distinguishable from chance—unlike the more robust and predictable behavior observed in CTRL animals (Figure S1 – data for individual animals; Table 1 – group level analysis and SSM reliability).

VPA-exposed animals exhibit increased choice perseveration

A common behavioral feature in individuals on the autism spectrum is a diminished ability to promptly perceive or respond to external stimuli, and to flexibly guide behavior based on changing circumstances. One potential manifestation of this is a failure to associate actions with their outcomes—such as associating a specific choice with the subsequent delivery or absence of a reward—and to adjust behavior, thus persevering in one particular trajectory regardless of reward contingencies.

To test this hypothesis, we analyzed raw DNMP data for signs of choice perseveration, operationalized as a persistent Left/Right Bias (LRB) during decision-making. Our analysis revealed a significant group effect: CTRL animals exhibited lower LRB compared to VPA-exposed groups (Figure 3; Table 2; GLMM: $\chi^2 = 13.63$, $p < 0.001$; Fixed Effect Omnibus test), indicating increased perseverative tendencies in VPA animals.

Further analysis revealed significant group-by-session interactions. While CTRL animals showed a reduction in LRB after the first DNMP session (S1)—suggesting adaptive learning and behavioral flexibility—both VPA groups (VP400 and VP600) maintained elevated LRB across multiple subsequent sessions. Specifically, compared to S1, significant LRB persistence was observed in VP400 and VP600 animals in sessions S2 (VP400: $p = 0.009$; VP600: $p = 0.041$) and S3 (VP400: $p = 0.035$; VP600: $p = 0.025$). In session S4, only VP400 animals continued to show a significant bias ($p = 0.048$), whereas VP600 animals did not (NS) (Figure 3; Table 2; GLMM: $\chi^2 = 13.63$, $p < 0.001$; Fixed Effect Omnibus test).

These findings support the notion that prenatal VPA exposure impairs the reduction of perseverative behavior across learning sessions. Unlike CTRL animals, VPA-exposed animals fail to flexibly adapt their choices based on past outcomes, consistent with behavioral inflexibility commonly observed in ASD.

40Hz sensory entrainment significantly increases gamma-frequency neural oscillations across brain regions

Functional imaging studies in individuals with ASD have consistently reported underconnectivity in parietal regions [14,15], while EEG data reveal disrupted gamma-band oscillations and reduced gamma coherence [16,17], as well as diminished fronto-temporal coherence in the 3–6 Hz range. Notably, the latter findings have shown responsiveness to sensory stimulation therapies [18–20]. In parallel, prenatal VPA exposure in rodent models leads to downregulation of Kv10.2 channel expression in the hippocampus, which results in elevated high-frequency oscillatory activity—a phenotype that can be reversed through compensatory gene overexpression [21]. These findings parallel MEG data in ASD patients showing increased power across delta, theta, alpha, and broadband gamma bands (20–120 Hz) in multiple cortical regions, including temporal, parietal, frontal, occipital, and midline areas, with stronger deviations associated with greater symptom severity [22,23]. Such gamma-frequency dysregulation is likely mediated by deficits in PV+ GABAergic interneurons, whose density is reduced in frontal, motor, and auditory cortices of ASD individuals (reviewed in [24]). Crucially, abnormal gamma oscillations in ASD patients have been shown to respond to behavioral interventions (e.g., PEERS) [25,26] and to transcranial stimulation protocols [27,28], resulting in durable improvements in both neural synchrony and behavior during adolescence. Based on this converging evidence, we hypothesized that auditory gamma-frequency sensory entrainment would mitigate the working memory (WM) deficits observed in VPA-exposed animals.

A wealth of evidence suggests that cortical networks in humans and animals can be reliably entrained to external stimuli—particularly light [29] and sound [30,31], delivered at gamma frequencies relevant to cognition. Recent rodent studies further demonstrate that 40 Hz gamma entrainment, via either visual or multimodal (visual and auditory) stimuli, improves cognitive function and induces broad changes in neuropathology and neuroplasticity in Alzheimer's disease models, with persistent effects following the intervention[32–36].

To test whether 40 Hz auditory stimulation could induce similar effects in the VPA rodent model, we recorded local field potentials (LFPs) in two animals—one VP600 and one CTRL—each implanted with multi-tetrode hyperdrives targeting the hippocampus and

cortical regions. During recording sessions, animals received 40 Hz patterned auditory stimulation, and their LFPs were analyzed using Fast Fourier Transform (FFT) and multi-taper spectral analysis [37]. Our analyses confirmed that auditory entrainment at 40 Hz enhances gamma-band power, as well as activity in other relevant frequency bands such as theta and beta (Figure 4). Importantly, we observed sustained changes in oscillatory power that persisted beyond the period of active stimulation. These results demonstrate that 40 Hz auditory stimulation effectively entrains neural circuits in awake, behaving rats, and induces lasting changes in neural dynamics, providing a possible mechanistic basis for therapeutic effects.

Auditory gamma entrainment restores working memory performance in VPA-exposed rats

Building on our finding that 40 Hz auditory stimulation reliably alters neural activity in both control and VPA-exposed animals, we next tested the therapeutic potential of this intervention on working memory (WM) deficits observed in VPA600 animals. To this end, a separate cohort of VPA600 animals was run through three consecutive sets of six DNMP sessions (Figure 5B). The middle block of sessions included auditory entrainment, delivered continuously throughout each behavioral session using a 40 Hz-patterned sound stimulus.

As shown in Figure 5A, auditory entrainment produced a robust and statistically significant improvement in DNMP performance across sessions. Specifically, performance during entrainment sessions was markedly enhanced compared to baseline: the average probability of a correct trial increased from 0.66 pre-entrainment to 0.78 during entrainment (GLMM, $p<0.001$). Strikingly, this performance was statistically indistinguishable from that of the CTRL animals (GLMM, $p = 0.497$), suggesting a full rescue of the WM deficit.

These findings were further supported by trial-by-trial analyses using both Binary Logistic Regression (Logit) and State-Space Modeling (SSM) (Figure 5C). During the entrainment sessions, VPA600 animals displayed trial-wise performance dynamics that closely resembled those of CTRL animals, with both methods showing increased and more consistent estimates of the probability of correct responses. These results strongly suggest that auditory gamma entrainment enhances WM performance to levels

comparable to those of unexposed controls. Please refer to Figure S1 for individual animals´ raw data and analysis.

VPA-exposed animals exhibit trajectory-perseverative behavior

Lastly, we investigated whether sensory entrainment (SE) also modulates perseverative behavior, operationalized as Left/Right Bias (LRB), in VPA-exposed animals. While LRB differences across pre-entrainment, entrainment, and post-entrainment sessions in the VP600 group were not statistically significant (Figure 6A, GLMM, $p = 0.068$), the data suggested a potential trend worth exploring further.

To contextualize this behavior and assess whether LRB presence or absence can emerge by chance during DNMP training, we used the original trial structure (i.e., blocked arm, trial count, group sizes, and sessions) to create seven replicates in which choice responses were randomly assigned from an unbiased distribution, allowing us to establish a comparison baseline, and thus assess the emergence and persistence of LRB across treatment groups (CTRL, VP400, and VP600 and VP600-entrainment).

Compared to synthetic data, CTRL animals exhibit LRB restricted to the first session, after which it becomes similar to levels resulting from synthetic data, in agreement with the previous data (Figure 6B). VP400 animals exhibited high LRB levels relative to the synthetic control group (Figure 6C, GLMM, group effect $p < 0.001$; session-by-group interaction $p = 0.597$, n.s.), with only modest attenuation across sessions ($p = 0.064$). VP600 animals showed similar results (GLMM, group effect $p < 0.001$; session-by-group interaction $p = 0.367$, n.s.), with a significant attenuation across sessions ($p = 0.004$).

Notably, sensory entrainment reduced LRB in VP600 animals (GLMM, entrainment effect $p = 0.004$; session effect $p = 0.003$; session-by-group interaction $p = 0.463$, n.s.). During entrainment sessions, LRB in VP600 animals was statistically indistinguishable from that of one of the synthetic replicates ($p = 0.229$) and significantly reduced compared to baseline sessions (individual session p values ranging from 0.001 to 0.013). These findings indicate that auditory gamma entrainment may transiently normalize perseverative tendencies, in addition to rescuing WM impairments.

Discussion

We have shown that prenatal exposure to Valproic Acid (VPA), a well-established rodent model of ASD, induces robust and persistent deficits in SWM performance in a delayed

non-match to place (DNMP) task. Importantly, we found that gamma-frequency sensory entrainment (SE) not only modulated neural activity in a frequency-specific and lasting manner but also rescued both cognitive and behavioral deficits in VPA-exposed animals.

Impaired WM and Learning Dynamics in VPA-Exposed Rats

Across sessions, VPA animals exhibited significantly poorer performance in the DNMP task compared to controls, with both VP400 and VP600 groups showing slower learning curves and reduced final performance levels. However, this impairment was not simply a reflection of delayed acquisition. Our trial-by-trial analyses using Binary Logistic Regression (BLR) and State Space Modeling (SSM) revealed that VPA animals lacked consistent within-session improvements and showed noisy or unstable probability estimates of correct responses, suggesting a fundamental disruption in the integration of recent experience to guide future choices.

This inability to progressively improve performance likely reflects underlying disruptions in distributed networks critical for goal-directed behavior (GDB), where allocentric representations must be reinstated from memory and translated into egocentric action plans [38–41]. This transformation relies on synchronized activity across the hippocampus (HIPP), posterior parietal cortex (PPC), retrosplenial cortex (RSC), and prefrontal areas—circuits known to be affected in ASD. Specifically, anatomical studies show increased local neuronal density and reduced long-range white matter connections in ASD brains, including decreased myelination and structural thinning of PPC, temporal, and frontal cortices [42–47]. These features are consistent with our behavioral findings and lend support to the hypothesis of impaired distributed coordination in ASD models.

Perseverative Behavior as a Signature of Cognitive Rigidity

Perseverative responding, quantified here as left/right bias (LRB), was significantly elevated in VPA-exposed animals and showed limited improvement with training - contrasting with the rapid reduction of LRB observed in control animals after session 1. This suggests that VPA animals struggle to update behavior considering changing contingencies, a form of cognitive rigidity common in ASD.

Such rigidity may stem from failures to integrate reinforcement signals with prior action choices. Indeed, ASD patients often show reduced flexibility in reversal learning tasks and diminished engagement of prefrontal-striatal circuits responsible for adaptive choice

updating. Moreover, abnormal connectivity patterns—such as reduced long-range frontoparietal coherence and increased local connectivity—have been extensively reported in ASD populations, potentially impairing the ability to coordinate goal-directed behaviors across functionally-relevant brain areas.

Restoring Function Through Gamma-Frequency Sensory Entrainment

Gamma-band oscillations (30–80 Hz) are thought to play a key role in coordinating distributed neural activity and enabling top-down control, attention, and WM maintenance. Disturbances in gamma rhythms are among the most robust electrophysiological findings in ASD, with reports of reduced gamma coherence and impaired phase locking to rhythmic stimuli in both EEG and MEG studies [14–17]. Notably, gamma oscillations are tightly regulated by PV+ GABAergic interneurons, which are reduced in number in several cortical regions in ASD [24].

In our study, auditory 40 Hz stimulation effectively entrained neural activity in behaving rats, enhancing not only gamma but also theta and beta band power. These changes persisted beyond stimulus exposure, suggesting durable network-level modulation. Importantly, when VPA600 animals were subjected to gamma entrainment during DNMP sessions, we observed a complete rescue of WM performance—rendering their performance statistically indistinguishable from that of controls. Trial-wise modeling further confirmed that entrained animals exhibited stabilized learning curves and trial probabilities, matching CTRL-like profiles.

Moreover, SE also attenuated perseverative bias in VPA600 animals, reducing LRB to levels indistinguishable from unbiased synthetic controls. This suggests that gamma entrainment not only improves task performance but may restore behavioral flexibility by re-engaging circuits underlying adaptive decision-making.

Mechanistic and Translational Implications

The beneficial effects of gamma entrainment observed here echo findings from Alzheimer's disease (AD) models, where 40 Hz sensory stimulation rescues cognitive performance and alters neuropathology. Similar interventions in ASD patients—such as transcranial stimulation and behavioral training - have shown promising results in normalizing gamma activity and improving cognitive and social function.

Our results suggest that gamma entrainment may counteract the “local-over-connectivity, long-range underconnectivity” pattern present in ASD by promoting coherent, distributed neural activity. This could facilitate the reinstatement of allocentric memory traces and enable more effective goal-directed action planning. Furthermore, entrainment may modulate PV+ interneuron function, stabilizing oscillatory regimes critical for SWM and behavioral flexibility.

Our findings demonstrate that prenatal VPA exposure impairs SWM and induces perseverative behavior in rats, reflecting key features of ASD. Trial-by-trial modeling reveals unstable learning dynamics in VPA animals, and the presence of persistent choice bias. However, auditory gamma-frequency sensory entrainment restores both cognitive performance and behavioral flexibility, offering a promising non-invasive intervention to modulate large-scale brain activity. These results support the hypothesis that rhythmic sensory stimulation may rescue functional deficits in ASD by restoring oscillatory coherence and long-range network coordination.

Acknowledgements

We are indebted to GIMM's Bioimaging, Comparative Pathology, and Rodent facilities for critical help. We want to thank all the members of the Lopes Lab for fruitful discussions and help.

FCT granted a PhD Fellowship (BD-202009547) to JC, and an Exploratory Grant (IF/00201/2013), an IMM Director's Fund Award, an Investigator FCT Position at IMM-JLA (IF/00201/2013), a Research Grant (PTDC/MED-NEU/29325/2017), the 2022.03699.CEECIND Coordinator Investigator contract to LVL, and the 2022.00811.CEECIND Principal Investigator contract to MR.

Author contributions

JC and MR designed the experiments, JC, ML and CM conducted the experiments, JC and MR analyzed the data, and JC, LL and MR wrote the manuscript.

Declaration of Interests

The authors declare no competing interests.

FIGURE LEGENDS

Figure 1. Delayed non-match to place (DNMP) performance in CTRL and VPA-exposed animals.

(A) Experimental design showing DNMP task protocol across six sessions (S1–S6).

(B) Average performance (probability of correct trials) across sessions for CTRL, VP400, and VP600 groups.

(C) Raw behavioral data from individual animals across all sessions. Error trials are marked red and correct trials green. Tick orientation corresponds to the maze arm choice (left vs right).

Figure 2. Trial-by-trial dynamics of performance in CTRL and VPA animals. State-space Modeling (darker shade) overlaid on Binary Logistic Regression (BLR) (light shade) trial-by-trial probability estimates, +/-95% CI showing average group-level performance over time, on each of the 6 DNMP sessions (individual plots), for CTRL (grey in panel A), VP400 (yellow in panel B) and VP600 (green in panel C) animals.

Figure 3. Choice perseveration (left/right bias, LRB) across groups and sessions. Group-level comparison of session-by-session LRB showing increased bias in VP400 and VP600 animals relative to CTRL (GLMM, $p<0.001$). CTRL animals exhibit a significant reduction of LRB after S1, while VPA groups retain elevated bias across sessions.

Figure 4. Neural entrainment to 40 Hz auditory stimulation in awake behaving rats. Power Spectral Density plots showing power changes at physiologically relevant frequencies under entrainment, often enduring beyond the entrainment stimulus delivery. (A) Auditory cortex, (B) Posterior Parietal cortex, (C) LPMR Thalamus, (D) Medial occipital secondary (Oc2M) cortex, (E) Hippocampal CA1 subfield during DNMP trials, raw data samples of the right panel.

Figure 5. Sensory entrainment (SE) rescues WM deficits in VPA600 animals.

(A) Group-level performance comparison during showing improved correct response rates during entrainment when compared to pre-entrainment ($p<0.001$), enduring into post-entrainment.

(B) Raw behavioral data from individual animals across all sessions (similar to Figure

1C), during the three epochs of the entrainment experiment: pre-entrainment (sessions 1–6), entrainment (sessions 7–12), and post-entrainment (sessions 13–18).

(C) Overlaid BLR (light shade) and SSM (strong shade) mean +/-95%CI, trial-wise estimates for VP600 animals, for the 6 sessions, across the three epochs of the experiment (similar to Figure 2). Entrainment epoch shows CTRL-like increases in trial-by-trial probability of correct responses. This improvement outlives the delivery of the entrainment stimulus, during post-entrainment.

Figure 6. Sensory entrainment reduces LRB in VPA600 animals.

(A) LRB scores across pre-entrainment, entrainment, and post-entrainment epochs in VP600 group.

(B) Comparison of CTRL levels with synthetic data shows a high LRB on Session1 followed by much lower levels, indistinguishable from unbiased simulations.

(C, D-left panel) LRB levels in VP400 and VP600 animals is significantly higher than that of synthetic data.

(D-right panel) LRB levels in VP600 animals decreases during entrainment, compared to synthetic data.

Methods

Lead Contact and Materials Availability

Further information and requests for resources and reagents should be directed to and will be fulfilled by the Lead Contact, Miguel Remondes, DVM, PhD (miguel.remondes@gimm.pt). This study did not generate new unique reagents.

Experimental Model Generation

All procedures were performed in accordance with EU and Institutional guidelines. Female and male rats aged 3-6 m, were obtained from Charles River France, kept in a 12hr light/dark cycle, fed *ad libitum*, housed in groups until mating cycles begun.

TIMED-MATING PROTOCOL

Pairs of males and females of the same age were formed, and single-caged.for 48 hours to reduce stress and prepare females for estrus synchronization. After the separation

period, cages were swapped between animals of the same pair to expose females to the scent of the male thus-timing estrus. Estrus was detected using periodic vaginal electrical impedance measurements. Once in peak estrus the pair was rejoined and allowed to mate overnight for a period of 8 hours. In the following morning, the pair was separated, and the female was inspected for the presence of a vaginal plug, in which case the female was labeled 'possibly pregnant' at day 0.5 (E0.5, embryonic day 5), and weighted daily thereafter.

VPA TREATMENT

Twelve days later, on E12.5, pregnant females received an IP injection of either saline (CTRL), 400 mg/ Kg (VP400), or 600 mg/ Kg (VP600) of valproic acid sodium salt (VPA, Sigma P4543) diluted in saline, and were housed individually. The day the pups were born was recorded as post-natal day 0 (P0), and the bedding was left undisturbed for 7 days. After weaning (P21), pups were housed in groups of up to 3 rats per cage, and assigned experimental groups according to treatment, CTRL (saline), VP400 (400 mg/ kg) and VP600 (600 mg/ kg).

DELAYED NON-MATCHING TO PLACE TASK

In preparation for the DNMP task, the above animals (now 6 month old) were food-restricted to 85% BW. The DNMP task was conducted in a T-maze featuring a starting platform (25x30 cm), a central corridor (170 cm) and two lateral exit arms (88 cm each) and whose ends a chocolate reward was placed. An external opaque resting box (57x39x42cm) was used to temporarily house the rat during the inter-trial maze setup. Each trial consisted in three runs: (1) Sample, (2) Delay and (3) Test. (1) Sample Run: one of the lateral arms (randomly defined) was baited with reward while the other arm was blocked. (2) After the rat visited the baited arm and consumed the reward, it was taken out of the maze and placed in the resting box for 20 seconds (the Delay). (3) Test Run: once the delay period had elapsed, the animal was returned to the maze, both whose lateral arms were accessible again. The rat was now rewarded for selecting the arm non-matching the one baited before (during Sample). Test trials were labelled accordingly Correct or Error. All sessions were recorded using a Flea 3 PointGreyTM at

30 fps acquisition rate (top view) mounted on a cable tray fixed on the ceiling above the T-maze and stored in the acquisition computer running Bonsai software.

Sound Entrainment Protocol

During the entrainment sessions a synthetically generated sound, consisting of a carrier tone of 8 kHz amplitude-modulated at 40 Hz, was continuously delivered by a speaker (Blow BT-950) placed inside the room, above and aligned with the T-maze central corridor, and modified until the Sound Pressure Level (SPL) reached 70 dB at the maze level.

Electrophysiological Recordings

Local field potential recordings were performed in awake-behaving CTRL and VP600 rats, using a multi-tetrode drive chronically implanted. The data was acquired at 20K sampling rate using Intan RHD2164 amplifier boards connected to the Open-Ephys board, as described earlier [48].

Behavioral Data Acquisition and Statistical Analysis

Trial outcomes were recorded ("correct" or "error") and classified as 0 or 1 across all groups, sessions and animals. Pooled, and, trial-by-trial data were analyzed using Matlab and Jamovi. The individual animals' behavior curve were computed for each individual session, from the individual trial outcomes, using two complementary methods: 1) State Space Model (SSM) [49] applied to estimate the individual subject learning curve using binomial expectation maximization and 2) a predictive binary logistic regression model. In both cases we computed the 95% confidence interval displayed in the main and supplementary plots, in both individual animals and groups. Generalized Linear Mixed Models (GLMM) were employed to analyze the behavioral outcome results. Model selection was based on the Akaike Information Criterion (AIC), with the chosen model being the one that converged and exhibited the lowest AIC value. To assess performance differences between VPA and CTRL groups, we used a GLMM with a binomial distribution and logit link function, with individual subjects as the random effects variable. The same GLMM, followed by a Bonferroni post-hoc test, was conducted to analyze the ratio of correct trials between groups during the experiment.

References

1. Scoville, W.B., Milner, B., and Scoville WB, M.B. (1957). Loss of recent memory after bilateral hippocampal lesions. J Neurol Neurosurg Psychiatry *20*, 11–21. https://doi.org/10.1136/jnnp.20.1.11.

2. NADEL, L. (1990). Varieties of Spatial Cognition: Psychobiological Considerations. Ann N Y Acad Sci *608*, 613–636. https://doi.org/10.1111/j.1749-6632.1990.tb48912.x.

3. Morris, R.G.M., Garrud, P., Rawlins, J.N.P., and O'Keefe, J. (1982). Place navigation impaired in rats with hippocampal lesions. Nature *297*, 681–683. https://doi.org/10.1038/297681a0.

4. DeLong, G.R. (1992). Autism, amnesia, hippocampus, and learning. Neurosci Biobehav Rev. https://doi.org/10.1016/S0149-7634(05)80052-1.

5. Ichim, A.M., Barzan, H., Moca, V.V., Nagy-Dabacan, A., Ciuparu, A., Hapca, A., Vervaeke, K., and Muresan, R.C. (2024). The gamma rhythm as a guardian of brain health. Elife *13*. https://doi.org/10.7554/ELIFE.100238.

6. Aggleton, J.P., Hunt, P.R., and Rawlins, J.N.P. (1986). The effects of hippocampal lesions upon spatial and non-spatial tests of working memory. Behavioural Brain Research *19*, 133–146. https://doi.org/10.1016/0166-4328(86)90011-2.

7. Shaw, C., and Aggleton, J.P. (1995). Evidence for the Independence of Recognition and Recency Memory in Amnesic Subjects. Cortex *31*, 57–71. https://doi.org/10.1016/S0010-9452(13)80105-0.

8. Maguire, E.A. (2001). Neuroimaging studies of autobiographical event memory. Philos Trans R Soc Lond B Biol Sci *356*, 1441–1451. https://doi.org/10.1098/RSTB.2001.0944).

9. Wilson, D.I.G., Langston, R.F., Schlesiger, M.I., Wagner, M., Watanabe, S., and Ainge, J.A. (2013). Lateral entorhinal cortex is critical for novel object-context recognition. Hippocampus *23*, 352–366. https://doi.org/10.1002/hipo.22095.

10. Shaw, C.L., Watson, G.D.R., Hallock, H.L., Cline, K.M., and Griffin, A.L. (2013). The role of the medial prefrontal cortex in the acquisition, retention, and reversal of a tactile visuospatial conditional discrimination task. Behavioural Brain Research *236*, 94–101. https://doi.org/10.1016/J.BBR.2012.08.024.

11. Mychasiuk, R., Richards, S., Nakahashi, A., Kolb, B., and Gibb, R. (2012). Effects of rat prenatal exposure to valproic acid on behaviour and neuro-anatomy. Dev Neurosci *34*, 268–276. https://doi.org/10.1159/000341786.

12. Pinto-Correia, B., Caldeira-Bernardo, P., and Remondes, M. (2024). Optogenetic silencing hippocampal inputs to the retrosplenial cortex causes a prolonged disruption of spatial working memory. https://doi.org/10.7554/elife.96515.2.

13. Cruz, A.S., Cruz, S., and Remondes, M. (2024). Effects of optogenetic silencing the anterior cingulate cortex in a delayed non-match to trajectory task. Oxford Open Neuroscience *3*. https://doi.org/10.1093/OONS/KVAE002.

14. Cherkassky, V.L., Kana, R.K., Keller, T.A., and Just, M.A. (2006). Functional connectivity in a baseline resting-state network in autism. Neuroreport *17*, 1687–1690. https://doi.org/10.1097/01.wnr.0000239956.45448.4c.

15. Just, M.A., Cherkassky, V.L., Keller, T.A., Kana, R.K., and Minshew, N.J. (2007). Functional and anatomical cortical underconnectivity in autism: evidence from an FMRI study of an executive function task and corpus callosum morphometry. Cereb Cortex *17*, 951–961. https://doi.org/10.1093/CERCOR/BHL006.

16. Brown, C., Gruber, T., Boucher, J., Rippon, G., and Brock, J. (2005). Gamma abnormalities during perception of illusory figures in autism. Cortex *41*, 364–376. https://doi.org/10.1016/s0010-9452(08)70273-9.

17. Rippon, G., Brock, J., Brown, C., and Boucher, J. (2007). Disordered connectivity in the autistic brain: challenges for the “new psychophysiology.” Int J Psychophysiol *63*, 164–172. https://doi.org/10.1016/J.IJPSYCHO.2006.03.012.

18. Murias, M., Webb, S.J., Greenson, J., and Dawson, G. (2007). Resting State Cortical Connectivity Reflected in EEG Coherence in Individuals With Autism. Biol Psychiatry *62*, 270–273. https://doi.org/10.1016/J.BIOPSYCH.2006.11.012.

19. Webb, S.J., Jones, E.J.H., Merkle, K., Venema, K., Greenson, J., Murias, M., and Dawson, G. (2011). Developmental Change in the ERP Responses to Familiar Faces in Toddlers With Autism Spectrum Disorders Versus Typical Development. Child Dev *82*, 1868–1886. https://doi.org/10.1111/j.1467-8624.2011.01656.x.

20. Dawson, G., Jones, E.J.H., Merkle, K., Venema, K., Lowy, R., Faja, S., Kamara, D., Murias, M., Greenson, J., Winter, J., et al. (2012). Early Behavioral Intervention Is Associated With Normalized Brain Activity in Young Children With Autism. J Am Acad Child Adolesc Psychiatry *51*, 1150–1159. https://doi.org/10.1016/J.JAAC.2012.08.018.

21. Wang, J., Feng, S., Li, M., Liu, Y., Yan, J., Tang, Y., Du, D., and Chen, F. (2019). Increased Expression of Kv10.2 in the Hippocampus Attenuates Valproic Acid-Induced Autism-Like Behaviors in Rats. Neurochem Res *44*, 2796–2808. https://doi.org/10.1007/S11064-019-02903-4.

22. Cornew, L., Roberts, T.P.L., Blaskey, L., and Edgar, J.C. (2012). Resting-state oscillatory activity in autism spectrum disorders. J Autism Dev Disord *42*, 1884–1894. https://doi.org/10.1007/S10803-011-1431-6/FIGURES/3.

23. Sun, L., Gru, C., Bo, S., Wibral, M., Tozman, T., Schlitt, S., Poustka, F., Singer, W., Freitag, C.M., Uhlhaas, P.J., et al. (2012). Impaired Gamma-Band Activity during Perceptual Organization in Adults with Autism Spectrum Disorders: Evidence for Dysfunctional Network Activity in Frontal-Posterior Cortices. The Journal of Neuroscience *32*, 9563–9573. https://doi.org/10.1523/jneurosci.1073-12.2012.

24. Rojas, D.C., and Wilson, L.B. (2014). γ-band abnormalities as markers of autism spectrum disorders. Preprint, https://doi.org/10.2217/bmm.14.15 https://doi.org/10.2217/bmm.14.15.

25. Baker, E., Veytsman, E., Martin, A.M., Blacher, J., and Stavropoulos, K.K.M. (2020). Increased Neural Reward Responsivity in Adolescents with ASD after Social Skills Intervention. Brain Sci *10*, 1–11. https://doi.org/10.3390/brainsci10060402.

26. Van Hecke, A.V., Stevens, S., Carson, A.M., Karst, J.S., Dolan, B., Schohl, K., McKindles, R.J., Remmel, R., and Brockman, S. (2015). Measuring the plasticity of social approach: a randomized controlled trial of the effects of the PEERS intervention on EEG asymmetry in adolescents with autism spectrum disorders. J Autism Dev Disord *45*, 316–335. https://doi.org/10.1007/S10803-013-1883-Y.

27. Sokhadze, E.M., El-Baz, A., Baruth, J., Mathai, G., Sears, L., and Casanova, M.F. (2009). Effects of low frequency repetitive transcranial magnetic stimulation (rTMS) on gamma frequency oscillations and event-related potentials during processing of illusory figures in autism. J Autism Dev Disord *39*, 619–634. https://doi.org/10.1007/S10803-008-0662-7.

28. Casanova, M.F., Shaban, M., Ghazal, M., El-Baz, A.S., Casanova, E.L., and Sokhadze, E.M. (2021). Ringing Decay of Gamma Oscillations and Transcranial Magnetic Stimulation Therapy in Autism Spectrum Disorder. Applied Psychophysiology Biofeedback *46*, 161–173. https://doi.org/10.1007/s10484-021-09509-z.

29. Cigánek, L. (1961). The EEG response (evoked potential) to light stimulus in man. Electroencephalogr Clin Neurophysiol *13*, 165–172. https://doi.org/10.1016/0013-4694(61)90132-8.

30. Galambos, R., Makeig, S., and Talmachoff, P.J. (1981). A 40-Hz auditory potential recorded from the human scalp. Proc Natl Acad Sci U S A *78*, 2643–2647. https://doi.org/10.1073/PNAS.78.4.2643.

31. Wang, X.-J., Abbott, LF., Blum, KI., Abbott, LF., Vreeswijk, C. van, Achard, S., Salvador, R., Whitcher, B., Suckling, J., Bullmore, E., et al. (2010). Neurophysiological and computational principles of cortical rhythms in cognition. Physiol Rev *90*, 1195–1268. https://doi.org/10.1152/physrev.00035.2008.

32. Martorell, A.J., Paulson, A.L., Suk, H.J., Abdurrob, F., Drummond, G.T., Guan, W., Young, J.Z., Kim, D.N.W., Kritskiy, O., Barker, S.J., et al. (2019). Multi-sensory Gamma Stimulation Ameliorates Alzheimer's-Associated Pathology and Improves Cognition. Cell *177*, 256-271.e22. https://doi.org/10.1016/J.CELL.2019.02.014.

33. Carlén, M., Meletis, K., Siegle, J.H., Cardin, J.A., Futai, K., Vierling-Claassen, D., Rühlmann, C., Jones, S.R., Deisseroth, K., Sheng, M., et al. (2012). A critical role for NMDA receptors in parvalbumin interneurons for gamma rhythm induction and behavior. Mol Psychiatry *17*, 537–548. https://doi.org/10.1038/mp.2011.31.

34. Cardin, J.A., Carlén, M., Meletis, K., Knoblich, U., Zhang, F., Deisseroth, K., Tsai, L.H., and Moore, C.I. (2009). Driving fast-spiking cells induces gamma rhythm and controls sensory responses. Nature *459*, 663–667. https://doi.org/10.1038/NATURE08002.

35. Canter, R.G., Penney, J., and Tsai, L.H. (2016). The road to restoring neural circuits for the treatment of Alzheimer's disease. Nature *539*, 187–196. https://doi.org/10.1038/NATURE20412.

36. Iaccarino, H.F., Singer, A.C., Martorell, A.J., Rudenko, A., Gao, F., Gillingham, T.Z., Mathys, H., Seo, J., Kritskiy, O., Abdurrob, F., et al. (2016). Gamma frequency entrainment attenuates amyloid load and modifies microglia. Nature *540*, 230–235. https://doi.org/10.1038/nature20587.

37. Bokil, H., Andrews, P., Kulkarni, J.E., Mehta, S., and Mitra, P.P. (2010). Chronux: A platform for analyzing neural signals. J Neurosci Methods *192*, 146–151. https://doi.org/10.1016/J.JNEUMETH.2010.06.020.

38. Michelmann, S., Price, A.R., Aubrey, B., Doyle, W.K., Friedman, D., Dugan, P., Devinsky, O., Devore, S., Flinker, A., Hasson, U., et al. (2020). Moment-by-moment tracking of naturalistic learning and its underlying hippocampo-cortical interactions. bioRxiv.

39. Gomez, A., Cerles, M., Rousset, S., Le Bas, J.-F., and Baciu, M. (2013). Ongoing egocentric spatial processing during learning of non-spatial information results in temporal-parietal activity during retrieval. Front Psychol *4*. https://doi.org/10.3389/fpsyg.2013.00366.

40. Burgess, N. (2008). Spatial cognition and the brain. Preprint at Blackwell Publishing Inc., https://doi.org/10.1196/annals.1440.002 https://doi.org/10.1196/annals.1440.002.

41. Gomez, A., Rousset, S., and Baciu, M. (2009). Egocentric-updating during navigation facilitates episodic memory retrieval. Acta Psychol (Amst) *132*, 221–227. https://doi.org/10.1016/j.actpsy.2009.07.003.

42. Casanova, M.F., Herbert, M.R., and Ziegler, D.A. (2004). White matter volume increase and minicolumns in autism [1] (multiple letters). Ann Neurol *56*, 453. https://doi.org/10.1002/ana.20196.

43. Buxhoeveden, D., Semendeferi, K., Buckwalter, J., Schenkar, N., Switzer, R., and Courchesne, E. (2006). Reduced minicolumns in the frontal cortex in patients with autism. Neuropathol. Appl. Neurobiol. *32*, 483–491.

44. Hadjikhani, N., Joseph, R.M., Snyder, J., and Tager-Flusberg, H. (2007). Abnormal activation of the social brain during face perception in autism. Hum. Brain Mapp. *28*, 441–449.

45. Abbott, A.E., Linke, A.C., Nair, A., Jahedi, A., Alba, L.A., Keown, C.L., Fishman, I., and Müller, R.A. (2018). Repetitive behaviors in autism are linked to imbalance of corticostriatal connectivity: a functional connectivity MRI study. Soc Cogn Affect Neurosci *13*, 32. https://doi.org/10.1093/SCAN/NSX129.

46. Herbert, M.R., Ziegler, D.A., Makris, N., Filipek, P.A., Kemper, T.L., Normandin, J.J., Sanders, H.A., Kennedy, D.N., and Caviness, V.S. (2004). Localization of white matter volume increase in autism and developmental language disorder. Ann Neurol *55*, 530–540. https://doi.org/10.1002/ANA.20032.

47. Kemper, T., and Bauman, M. (1998). Neuropathology of infantile autism. J. Neuropathol. Exp. Neurol. *57*, 645–652.

48. Dias, M., Ferreira, R., and Remondes, M. (2021). Medial Entorhinal Cortex Excitatory Neurons Are Necessary for Accurate Timing. Journal of Neuroscience *41*, 9932–9943. https://doi.org/10.1523/JNEUROSCI.0750-21.2021.

49. Suzuki, W.A., and Brown, E.N. (2005). Analyses of Dynamic Learning Processes. *4*. https://doi.org/10.1177/1534582305280030.

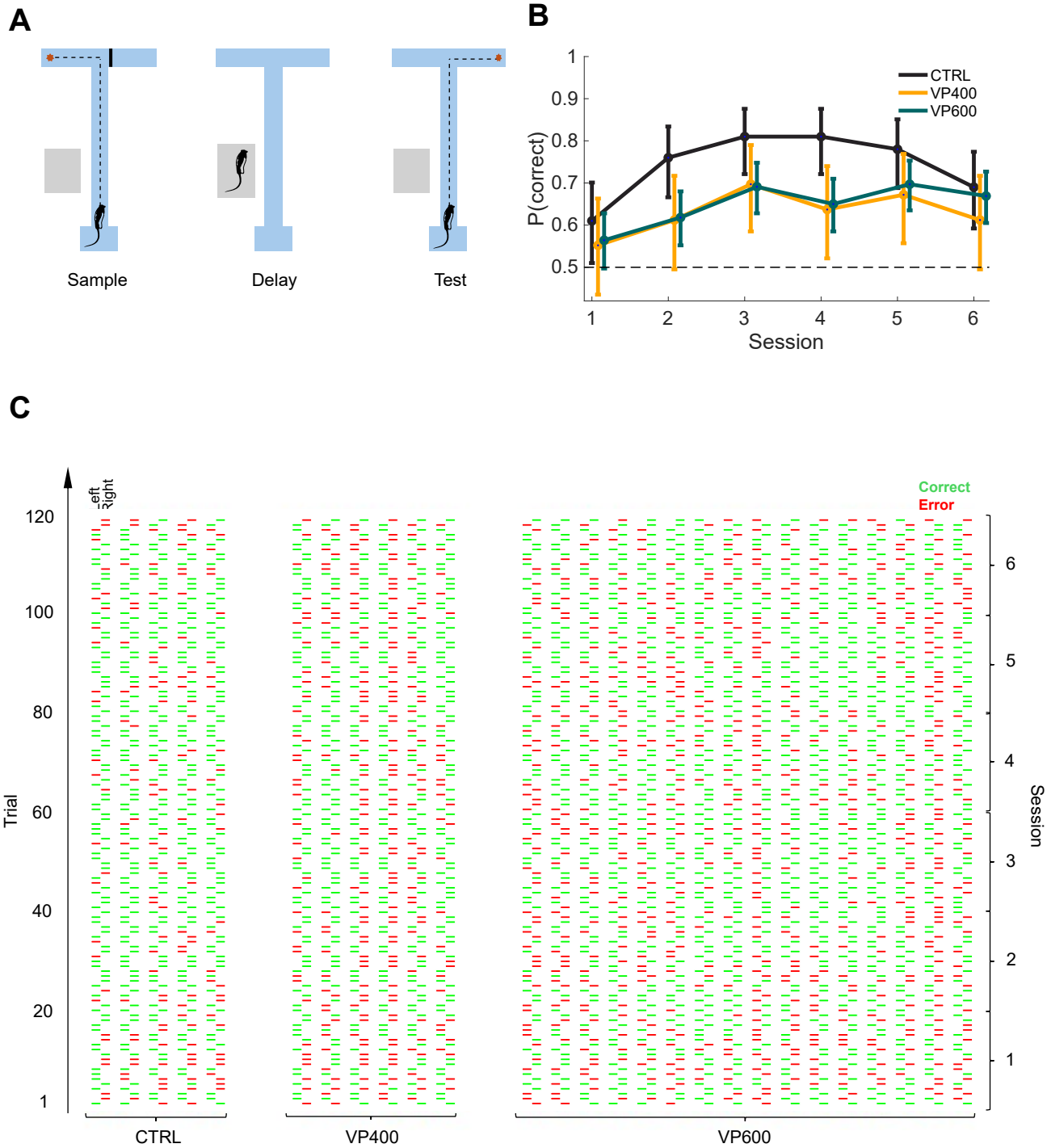
A
Sample
Delay
Test
B
P(correct)
Session
CTRL
VP400
VP600
C
Left
Right
Correct
Error
Trial
Session
CTRL
VP400
VP600

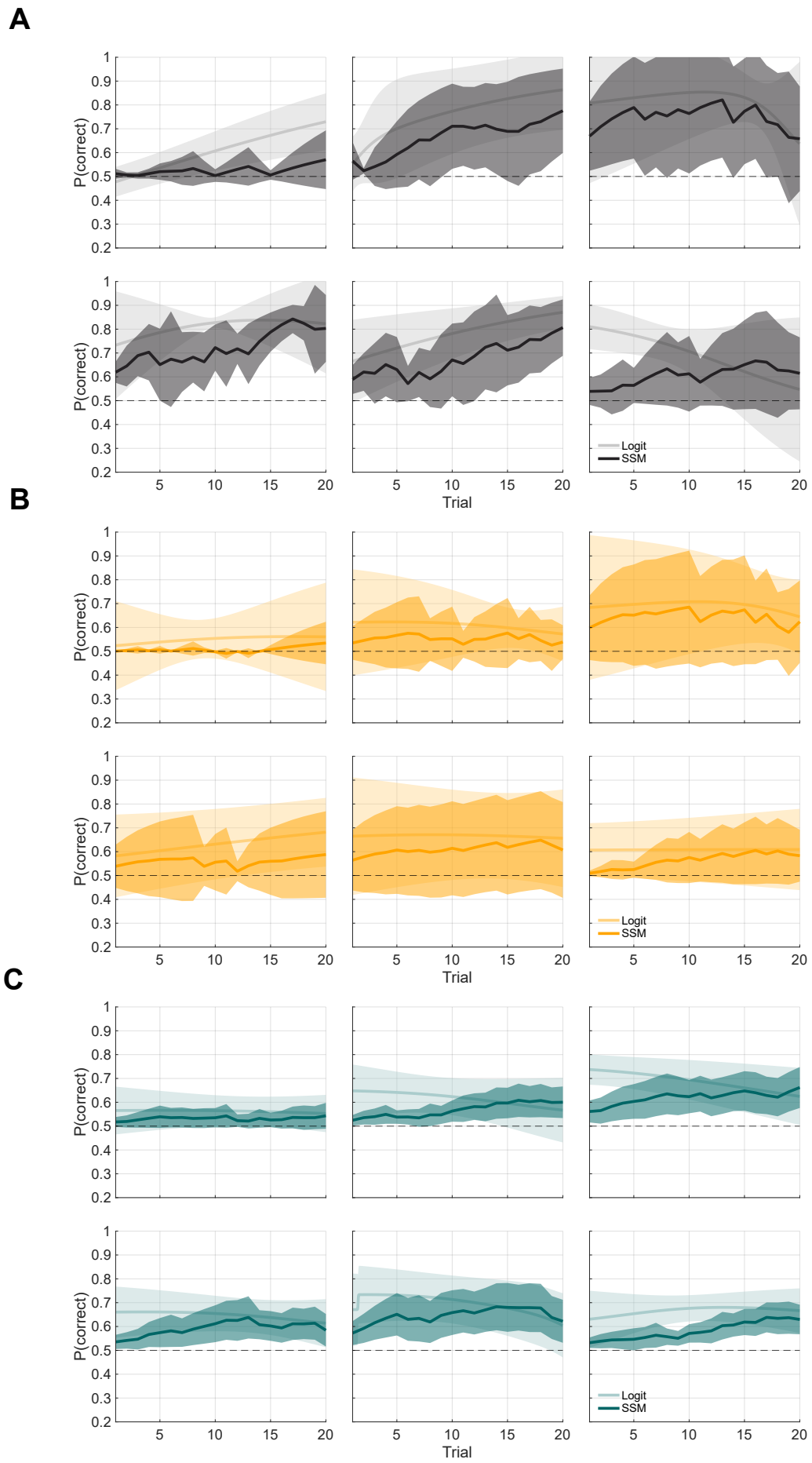
A
B
C
P(correct)
Trial
Logit
SSM

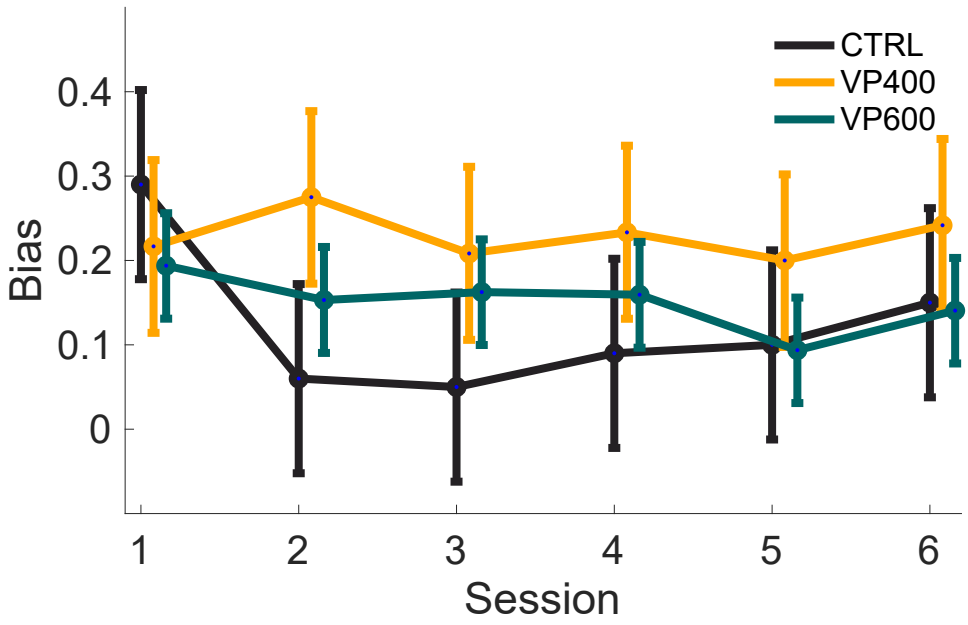
CTRL
VP400
VP600
0.4
0.3
0.2
0.1
0
Bias
1
2
3
4
5
6
Session

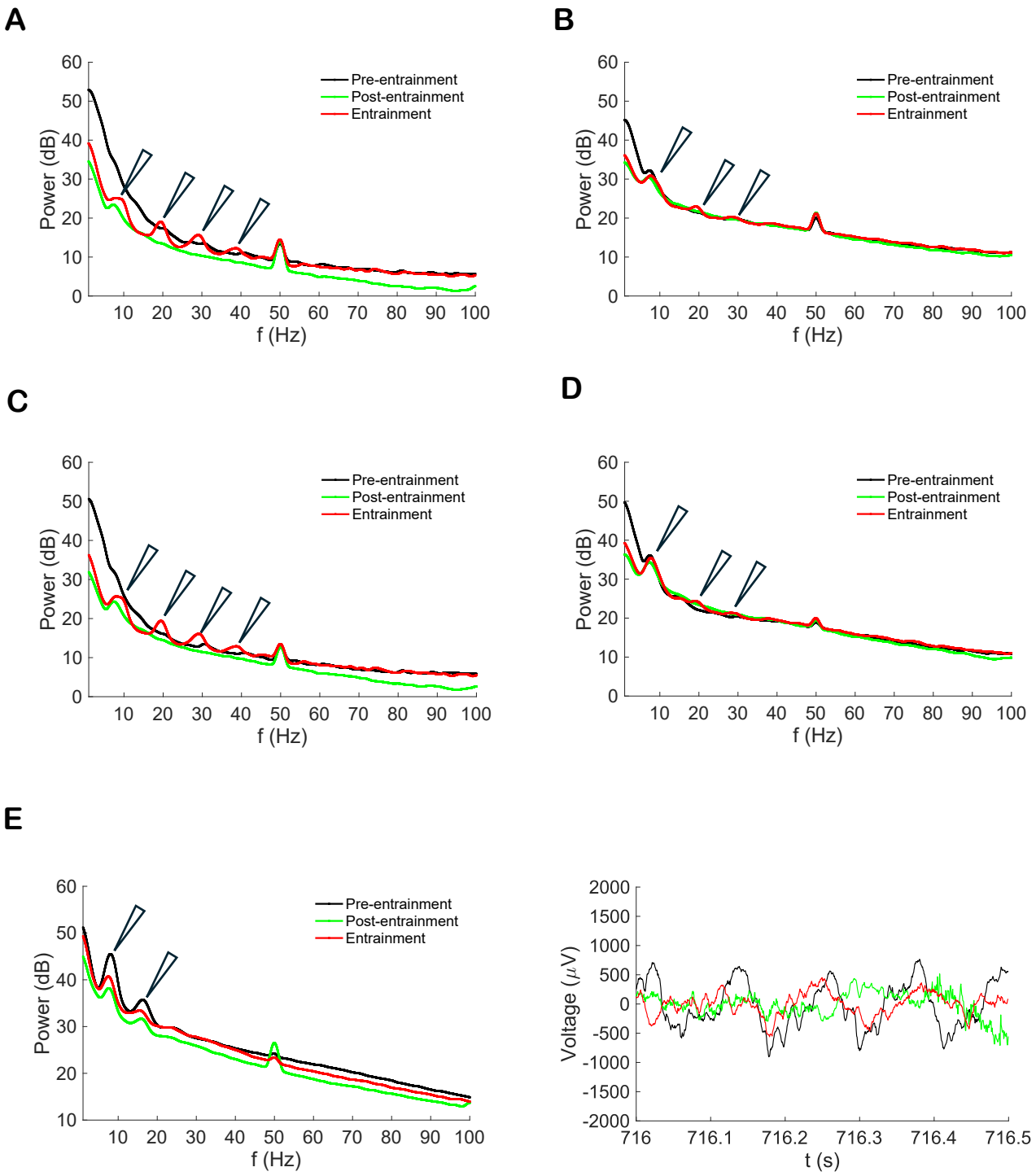
A
B
C
D
E
Pre-entrainment
Post-entrainment
Entrainment
Power (dB)
f (Hz)
Voltage (μV)
t (s)

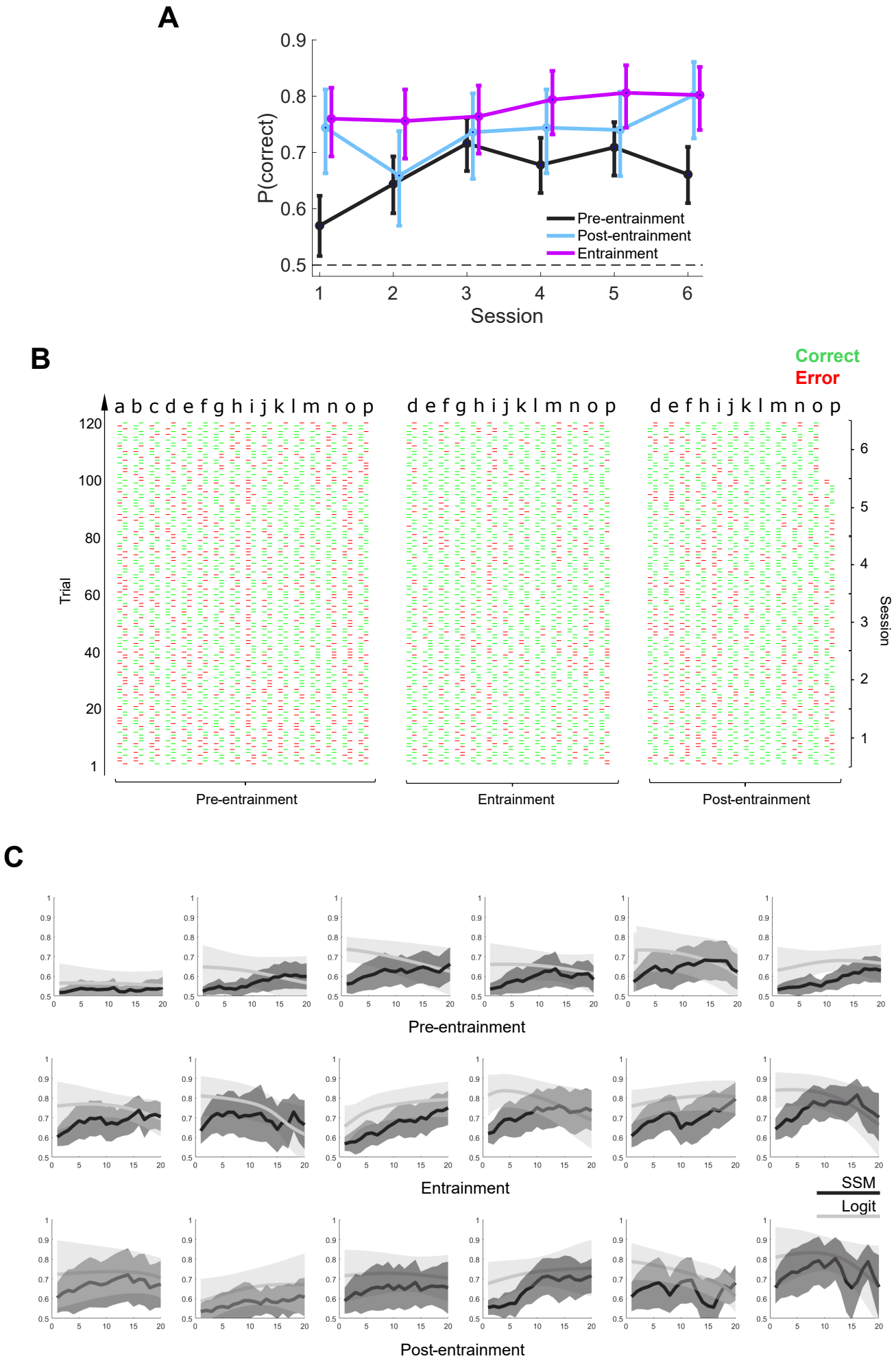
A
P(correct)
Session
Pre-entrainment
Post-entrainment
Entrainment
B
Correct
Error
Trial
Session
Pre-entrainment
Entrainment
Post-entrainment
C
Pre-entrainment
Entrainment
Post-entrainment
SSM
Logit

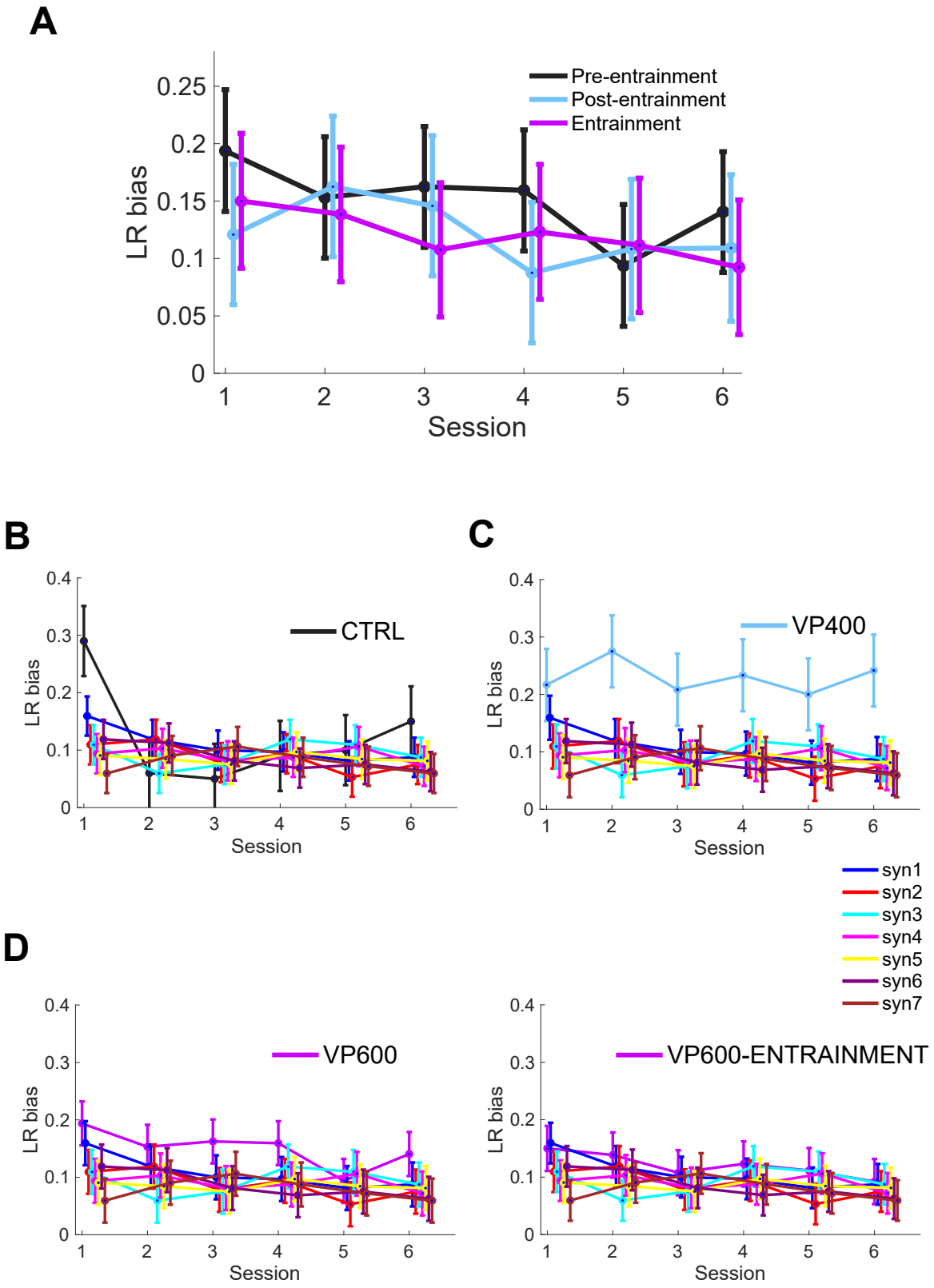
A
Pre-entrainment
Post-entrainment
Entrainment
LR bias
Session
B
CTRL
C
VP400
D
VP600
VP600-ENTRAINMENT
syn1
syn2
syn3
syn4
syn5
syn6
syn7

NUMBER OF SESSIONS FOR EACH ANIMAL

CTRL

	CTRL MRE313	CTRL MRE315	CTRL MRE325	CTRL MRE326	CTRL MRE327
95%CI clears					
50%	4	4	3	3	2
SSM stable	5	6	4	4	5

VPA 400 mg

	V400 MRE341	V400 MRE342	V400 MRE343	V400 MRE344	V400 MRE345	V400 MRE346
95%CI clears						
50%	1	2	0	0	1	2
SSM stable	5	3	0	0	2	4

VPA 600 mg

	V600 MRE378	V600 MRE379	V600 MRE380	V600 MRE389	V600 MRE390	V600 MRE391	V600 MRE392
95%CI clears							
50%	0	3	0	0	2	1	4
SSM stable	3	3	3	4	3	2	6

	V600 MRE393	V600 MRE394	V600 MRE407	V600 MRE408	V600 MRE409	V600 MRE410	V600 MRE412	V600 MRE413	V600 MRE468
95%CI clears									
50%	2	0	1	0	1	4	2	0	2
SSM stable	3	0	3	4	4	4	4	2	3

Analysis 01 - Comparing CTL's, V400 and V600 groups

Generalized Mixed Model

Model Info

Info	Value	Comment
Model Type	Logistic	Model for binary y
Call	glm	BinaryTrialOutcome ~ 1 + Group + Session + Group:Session + (1 + Group | Rat)
Link function	Logit	Log of the odd of y=1 over y=0
Direction	P(y=1)/P(y=0)	P(BinaryTrialOutcome = 1) / P(BinaryTrialOutcome = 0)
Distribution	Binomial	Dichotomous event distribution of y
LogLikel.	-2030.3641	Unconditional Log-Likelihood
-2*LogLikel.	4060.7282	Unconditional absolute deviance
Deviance	4014.7748	Conditional relative deviance
R-squared	0.0276	Marginal
R-squared	0.0522	Conditional
AIC	4108.7300	Less is better
BIC	4254.7281	Less is better
Residual DF	3216.0000	
Chi-squared/DF	0.9942	Overdispersion indicator
Converged	yes	
Optimizer	bobyqa	

[3]

Model Results

Fixed Effect Omnibus tests

	X^2	df	p
Group	15.05	2.00	<.001
Session	30.79	5.00	<.001
Group ✻ Session	6.83	10.00	0.742

Fixed Effects Parameter Estimates

Names	Effect	Estimate	SE	exp(B)	95% Exp(B) Confidence Interval		z	p
					Lower	Upper		
(Intercept)	(Intercept)	0.7501	0.0725	2.117	1.837	2.440	10.346	<.001
Group1	V400 - CTL	-0.5572	0.1981	0.573	0.389	0.844	-2.814	0.005
Group2	V600 - CTL	-0.4789	0.1352	0.619	0.475	0.807	-3.541	<.001
Session1	2 - 1	0.3927	0.1469	1.481	1.110	1.975	2.673	0.008
Session2	3 - 1	0.7263	0.1527	2.067	1.533	2.789	4.755	<.001
Session3	4 - 1	0.5742	0.1512	1.776	1.320	2.388	3.797	<.001
Session4	5 - 1	0.6353	0.1497	1.888	1.408	2.531	4.243	<.001
Session5	6 - 1	0.3491	0.1442	1.418	1.069	1.881	2.422	0.015
Group1 ✻ Session1	V400 - CTL ✻ 2 - 1	-0.4585	0.4095	0.632	0.283	1.411	-1.120	0.263
Group2 ✻ Session1	V600 - CTL ✻ 2 - 1	-0.4816	0.3511	0.618	0.310	1.230	-1.371	0.170
Group1 ✻ Session2	V400 - CTL ✻ 3 - 1	-0.3770	0.4266	0.686	0.297	1.583	-0.884	0.377
Group2 ✻ Session2	V600 - CTL ✻ 3 - 1	-0.4551	0.3672	0.634	0.309	1.303	-1.239	0.215
Group1 ✻ Session3	V400 - CTL ✻ 4 - 1	-0.6464	0.4228	0.524	0.229	1.200	-1.529	0.126
Group2 ✻ Session3	V600 - CTL ✻ 4 - 1	-0.6419	0.3660	0.526	0.257	1.078	-1.754	0.079
Group1 ✻ Session4	V400 - CTL ✻ 5 - 1	-0.3108	0.4168	0.733	0.324	1.659	-0.746	0.456
Group2 ✻ Session4	V600 - CTL ✻ 5 - 1	-0.2408	0.3582	0.786	0.390	1.586	-0.672	0.501
Group1 ✻ Session5	V400 - CTL ✻ 6 - 1	-0.1056	0.3995	0.900	0.411	1.969	-0.264	0.791
Group2 ✻ Session5	V600 - CTL ✻ 6 - 1	0.0934	0.3407	1.098	0.563	2.141	0.274	0.784

Random Components

Groups	Name	SD	Variance	ICC
Rat	(Intercept)	0.0302	9.11e-4	2.77e-4
	Group1	0.4014	0.1611	
	Group2	0.2804	0.0786	
Residuals		1.0000	1.0000	.

Note. Number of Obs: 3240 , groups: Rat 27

Random Parameters correlations

Groups	Param.1	Param.2	Corr.
Rat	(Intercept)	Group1	0.339
	(Intercept)	Group2	-0.566
	Group1	Group2	-0.934

Post Hoc Tests

Post Hoc Comparisons - Group

Comparison						
Group		**Group**	**exp(B)**	**SE**	**z**	**$p_{bonferroni}$**
CTL	-	V400	1.746	0.346	2.814	0.015
CTL	-	V600	1.614	0.218	3.541	0.001
V400	-	V600	0.925	0.178	-0.407	1.000

Post Hoc Comparisons - Session

Comparison						
Session		**Session**	**exp(B)**	**SE**	**z**	**$p_{bonferroni}$**
1	-	2	0.675	0.0992	-2.673	0.113
1	-	3	0.484	0.0739	-4.755	<.001
1	-	4	0.563	0.0852	-3.797	0.002
1	-	5	0.530	0.0793	-4.243	<.001
1	-	6	0.705	0.1017	-2.422	0.232
2	-	3	0.716	0.1131	-2.112	0.520
2	-	4	0.834	0.1305	-1.160	1.000
2	-	5	0.785	0.1216	-1.565	1.000
2	-	6	1.045	0.1563	0.291	1.000
3	-	4	1.164	0.1885	0.939	1.000
3	-	5	1.095	0.1758	0.567	1.000
3	-	6	1.458	0.2265	2.428	0.228
4	-	5	0.941	0.1497	-0.384	1.000
4	-	6	1.252	0.1927	1.463	1.000
5	-	6	1.331	0.2029	1.878	0.906

Post Hoc Comparisons - Group ✻ Session

Comparison							
Group	Session		Group	Session	exp(B)	SE	z	$p_{bonferroni}$
CTL	1	-	CTL	2	0.494	0.1536	-2.26862	1.000
CTL	1	-	CTL	3	0.367	0.1199	-3.06745	0.330
CTL	1	-	CTL	4	0.367	0.1199	-3.06765	0.330
CTL	1	-	CTL	5	0.441	0.1396	-2.58581	1.000
CTL	1	-	CTL	6	0.702	0.2093	-1.18518	1.000
CTL	1	-	V400	1	1.272	0.4033	0.75970	1.000
CTL	1	-	V400	2	0.993	0.3171	-0.02113	1.000
CTL	1	-	V400	3	0.680	0.2214	-1.18455	1.000
CTL	1	-	V400	4	0.890	0.2854	-0.36303	1.000
CTL	1	-	V400	5	0.765	0.2473	-0.82787	1.000
CTL	1	-	V400	6	0.993	0.3170	-0.02114	1.000
CTL	1	-	V600	1	1.211	0.3006	0.77028	1.000
CTL	1	-	V600	2	0.967	0.2412	-0.13344	1.000
CTL	1	-	V600	3	0.700	0.1763	-1.41747	1.000
CTL	1	-	V600	4	0.843	0.2111	-0.68088	1.000
CTL	1	-	V600	5	0.679	0.1714	-1.53380	1.000
CTL	1	-	V600	6	0.775	0.1945	-1.01690	1.000
CTL	2	-	CTL	3	0.743	0.2571	-0.85945	1.000
CTL	2	-	CTL	4	0.743	0.2571	-0.85952	1.000
CTL	2	-	CTL	5	0.893	0.3004	-0.33617	1.000
CTL	2	-	CTL	6	1.423	0.4537	1.10696	1.000
CTL	2	-	V400	2	2.012	0.6816	2.06486	1.000
CTL	2	-	V400	3	1.378	0.4750	0.92896	1.000
CTL	2	-	V400	4	1.803	0.6133	1.73395	1.000
CTL	2	-	V400	5	1.550	0.5310	1.28040	1.000
CTL	2	-	V400	6	2.012	0.6816	2.06472	1.000
CTL	2	-	V600	2	1.960	0.5368	2.45626	1.000
CTL	2	-	V600	3	1.417	0.3917	1.26191	1.000
CTL	2	-	V600	4	1.709	0.4695	1.94915	1.000
CTL	2	-	V600	5	1.376	0.3807	1.15272	1.000
CTL	2	-	V600	6	1.570	0.4324	1.63641	1.000
CTL	3	-	CTL	4	1.000	0.3606	1.48e-5	1.000
CTL	3	-	CTL	5	1.203	0.4223	0.52531	1.000
CTL	3	-	CTL	6	1.916	0.6408	1.94535	1.000
CTL	3	-	V400	3	1.855	0.6665	1.71976	1.000
CTL	3	-	V400	4	2.428	0.8614	2.50118	1.000
CTL	3	-	V400	5	2.088	0.7454	2.06156	1.000
CTL	3	-	V400	6	2.710	0.9577	2.82069	0.733
CTL	3	-	V600	3	1.909	0.5616	2.19658	1.000
CTL	3	-	V600	4	2.301	0.6735	2.84604	0.677
CTL	3	-	V600	5	1.852	0.5456	2.09319	1.000
CTL	3	-	V600	6	2.113	0.6201	2.55075	1.000
CTL	4	-	CTL	5	1.203	0.4223	0.52528	1.000
CTL	4	-	CTL	6	1.916	0.6408	1.94529	1.000
CTL	4	-	V400	4	2.428	0.8614	2.50119	1.000
CTL	4	-	V400	5	2.088	0.7454	2.06154	1.000
CTL	4	-	V400	6	2.710	0.9577	2.82061	0.733
CTL	4	-	V600	4	2.301	0.6735	2.84603	0.677
CTL	4	-	V600	5	1.852	0.5456	2.09314	1.000
CTL	4	-	V600	6	2.113	0.6201	2.55074	1.000
CTL	5	-	CTL	6	1.594	0.5166	1.43731	1.000
CTL	5	-	V400	5	1.736	0.6033	1.58723	1.000
CTL	5	-	V400	6	2.253	0.7747	2.36304	1.000

Post Hoc Comparisons - Group ✻ Session

Comparison							
Group	Session		Group	Session	exp(B)	SE	z	$p_{bonferroni}$
CTL	5	-	V600	5	1.540	0.4358	1.52709	1.000
CTL	5	-	V600	6	1.757	0.4951	2.00151	1.000
CTL	6	-	V400	6	1.414	0.4617	1.06105	1.000
CTL	6	-	V600	6	1.103	0.2872	0.37601	1.000
V400	1	-	CTL	2	0.388	0.1306	-2.81220	0.753
V400	1	-	CTL	3	0.288	0.1013	-3.54039	0.061
V400	1	-	CTL	4	0.288	0.1013	-3.53992	0.061
V400	1	-	CTL	5	0.346	0.1184	-3.10064	0.295
V400	1	-	CTL	6	0.552	0.1791	-1.83070	1.000
V400	1	-	V400	2	0.781	0.2078	-0.93017	1.000
V400	1	-	V400	3	0.534	0.1464	-2.28804	1.000
V400	1	-	V400	4	0.700	0.1874	-1.33355	1.000
V400	1	-	V400	5	0.601	0.1630	-1.87644	1.000
V400	1	-	V400	6	0.781	0.2078	-0.93020	1.000
V400	1	-	V600	1	0.952	0.2627	-0.17956	1.000
V400	1	-	V600	2	0.760	0.2106	-0.98950	1.000
V400	1	-	V600	3	0.550	0.1537	-2.14035	1.000
V400	1	-	V600	4	0.663	0.1842	-1.48007	1.000
V400	1	-	V600	5	0.534	0.1493	-2.24477	1.000
V400	1	-	V600	6	0.609	0.1696	-1.78118	1.000
V400	2	-	CTL	3	0.369	0.1304	-2.82069	0.733
V400	2	-	CTL	4	0.369	0.1304	-2.82059	0.733
V400	2	-	CTL	5	0.444	0.1526	-2.36303	1.000
V400	2	-	CTL	6	0.707	0.2309	-1.06099	1.000
V400	2	-	V400	3	0.685	0.1890	-1.37243	1.000
V400	2	-	V400	4	0.896	0.2422	-0.40567	1.000
V400	2	-	V400	5	0.770	0.2105	-0.95434	1.000
V400	2	-	V400	6	1.000	0.2686	-1.08e−5	1.000
V400	2	-	V600	2	0.974	0.2721	-0.09495	1.000
V400	2	-	V600	3	0.704	0.1985	-1.24376	1.000
V400	2	-	V600	4	0.849	0.2380	-0.58404	1.000
V400	2	-	V600	5	0.684	0.1929	-1.34820	1.000
V400	2	-	V600	6	0.780	0.2191	-0.88470	1.000
V400	3	-	CTL	4	0.539	0.1937	-1.71975	1.000
V400	3	-	CTL	5	0.648	0.2268	-1.23889	1.000
V400	3	-	CTL	6	1.033	0.3439	0.09781	1.000
V400	3	-	V400	4	1.309	0.3637	0.96968	1.000
V400	3	-	V400	5	1.125	0.3159	0.42119	1.000
V400	3	-	V400	6	1.461	0.4034	1.37241	1.000
V400	3	-	V600	3	1.029	0.2975	0.09841	1.000
V400	3	-	V600	4	1.240	0.3568	0.74852	1.000
V400	3	-	V600	5	0.999	0.2891	-0.00474	1.000
V400	3	-	V600	6	1.139	0.3285	0.45255	1.000
V400	4	-	CTL	5	0.495	0.1709	-2.03611	1.000
V400	4	-	CTL	6	0.789	0.2588	-0.72204	1.000
V400	4	-	V400	5	0.860	0.2364	-0.54981	1.000
V400	4	-	V400	6	1.116	0.3016	0.40566	1.000
V400	4	-	V600	4	0.947	0.2671	-0.19171	1.000
V400	4	-	V600	5	0.763	0.2165	-0.95402	1.000
V400	4	-	V600	6	0.870	0.2459	-0.49152	1.000
V400	5	-	CTL	6	0.918	0.3034	-0.25916	1.000
V400	5	-	V400	6	1.298	0.3547	0.95434	1.000
V400	5	-	V600	5	0.887	0.2544	-0.41712	1.000

Post Hoc Comparisons - Group ✻ Session

Comparison								
Group	Session		Group	Session	exp(B)	SE	z	$p_{bonferroni}$
V400	5	-	V600	6	1.012	0.2890	0.04294	1.000
V400	6	-	V600	6	0.780	0.2191	-0.88470	1.000
V600	1	-	CTL	2	0.408	0.1113	-3.28693	0.155
V600	1	-	CTL	3	0.303	0.0881	-4.10532	0.006
V600	1	-	CTL	4	0.303	0.0881	-4.10530	0.006
V600	1	-	CTL	5	0.364	0.1017	-3.61766	0.045
V600	1	-	CTL	6	0.580	0.1495	-2.11238	1.000
V600	1	-	V400	2	0.820	0.2285	-0.71093	1.000
V600	1	-	V400	3	0.562	0.1606	-2.01819	1.000
V600	1	-	V400	4	0.735	0.2060	-1.09808	1.000
V600	1	-	V400	5	0.632	0.1789	-1.62068	1.000
V600	1	-	V400	6	0.820	0.2285	-0.71094	1.000
V600	1	-	V600	2	0.799	0.1299	-1.38044	1.000
V600	1	-	V600	3	0.578	0.0963	-3.28971	0.153
V600	1	-	V600	4	0.696	0.1143	-2.20398	1.000
V600	1	-	V600	5	0.561	0.0938	-3.45837	0.083
V600	1	-	V600	6	0.640	0.1057	-2.70275	1.000
V600	2	-	CTL	3	0.379	0.1106	-3.32395	0.136
V600	2	-	CTL	4	0.379	0.1106	-3.32386	0.136
V600	2	-	CTL	5	0.456	0.1277	-2.80460	0.771
V600	2	-	CTL	6	0.726	0.1879	-1.23644	1.000
V600	2	-	V400	3	0.703	0.2016	-1.22895	1.000
V600	2	-	V400	4	0.920	0.2587	-0.29570	1.000
V600	2	-	V400	5	0.791	0.2247	-0.82490	1.000
V600	2	-	V400	6	1.027	0.2869	0.09494	1.000
V600	2	-	V600	3	0.723	0.1217	-1.92604	1.000
V600	2	-	V600	4	0.872	0.1444	-0.82814	1.000
V600	2	-	V600	5	0.702	0.1184	-2.09730	1.000
V600	2	-	V600	6	0.801	0.1335	-1.33167	1.000
V600	3	-	CTL	4	0.524	0.1542	-2.19653	1.000
V600	3	-	CTL	5	0.630	0.1781	-1.63417	1.000
V600	3	-	CTL	6	1.004	0.2624	0.01570	1.000
V600	3	-	V400	4	1.272	0.3607	0.84977	1.000
V600	3	-	V400	5	1.094	0.3133	0.31339	1.000
V600	3	-	V400	6	1.420	0.4002	1.24378	1.000
V600	3	-	V600	4	1.205	0.2045	1.10158	1.000
V600	3	-	V600	5	0.971	0.1675	-0.17281	1.000
V600	3	-	V600	6	1.107	0.1890	0.59766	1.000
V600	4	-	CTL	5	0.523	0.1469	-2.30801	1.000
V600	4	-	CTL	6	0.833	0.2163	-0.70379	1.000
V600	4	-	V400	5	0.907	0.2585	-0.34090	1.000
V600	4	-	V400	6	1.178	0.3301	0.58404	1.000
V600	4	-	V600	5	0.805	0.1370	-1.27383	1.000
V600	4	-	V600	6	0.919	0.1545	-0.50466	1.000
V600	5	-	CTL	6	1.035	0.2707	0.12968	1.000
V600	5	-	V400	6	1.463	0.4127	1.34820	1.000
V600	5	-	V600	6	1.141	0.1953	0.77028	1.000

Estimated Marginal Means

Group

				95% Confidence Interval	
Group	**Prob.**	**SE**	**df**	**Lower**	**Upper**
CTL	0.749	0.0190	Inf	0.710	0.785
V400	0.631	0.0396	Inf	0.551	0.705
V600	0.649	0.0205	Inf	0.608	0.688

Session

				95% Confidence Interval	
Session	**Prob.**	**SE**	**df**	**Lower**	**Upper**
1	0.575	0.0281	Inf	0.520	0.629
2	0.667	0.0271	Inf	0.612	0.718
3	0.737	0.0250	Inf	0.685	0.783
4	0.706	0.0264	Inf	0.652	0.755
5	0.719	0.0253	Inf	0.667	0.766
6	0.658	0.0267	Inf	0.604	0.708

Group:Session

					95% Confidence Interval	
Group	**Session**	**Prob.**	**SE**	**df**	**Lower**	**Upper**
CTL	1	0.610	0.0493	Inf	0.510	0.701
V400	1	0.552	0.0593	Inf	0.435	0.663
V600	1	0.564	0.0336	Inf	0.497	0.628
CTL	2	0.760	0.0431	Inf	0.666	0.834
V400	2	0.612	0.0576	Inf	0.495	0.717
V600	2	0.618	0.0327	Inf	0.552	0.680
CTL	3	0.810	0.0395	Inf	0.721	0.876
V400	3	0.697	0.0530	Inf	0.585	0.790
V600	3	0.691	0.0306	Inf	0.628	0.748
CTL	4	0.810	0.0395	Inf	0.721	0.876
V400	4	0.637	0.0565	Inf	0.521	0.740
V600	4	0.650	0.0319	Inf	0.585	0.710
CTL	5	0.780	0.0418	Inf	0.688	0.851
V400	5	0.672	0.0547	Inf	0.557	0.769
V600	5	0.697	0.0304	Inf	0.635	0.753
CTL	6	0.690	0.0467	Inf	0.592	0.774
V400	6	0.612	0.0576	Inf	0.495	0.717
V600	6	0.669	0.0314	Inf	0.605	0.727

Effects Plots

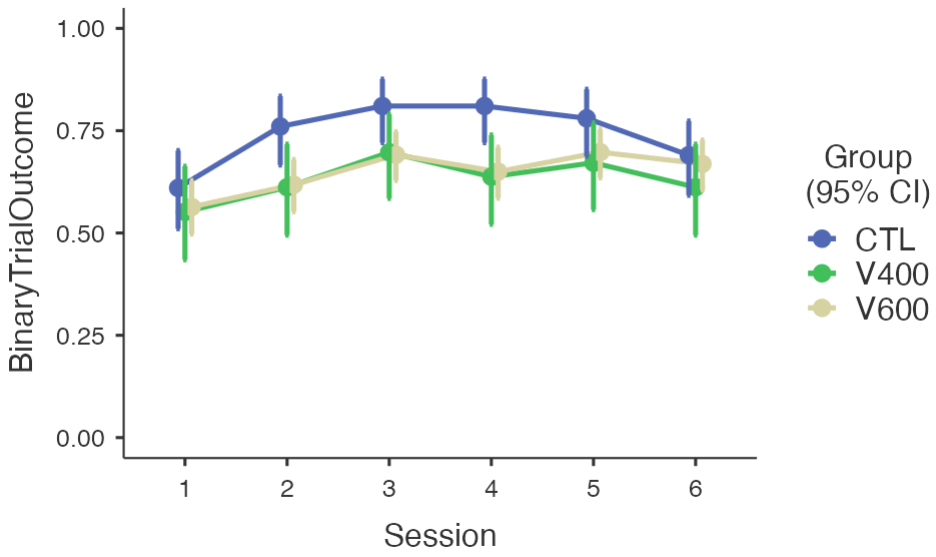

References

[1] The jamovi project (2022). *jamovi*. (Version 2.3) [Computer Software]. Retrieved from https://www.jamovi.org.

[2] R Core Team (2021). *R: A Language and environment for statistical computing*. (Version 4.1) [Computer software]. Retrieved from https://cran.r-project.org. (R packages retrieved from MRAN snapshot 2022-01-01).

[3] Gallucci, M. (2019). *GAMLj: General analyses for linear models*. [jamovi module]. Retrieved from https://gamlj.github.io/.

Analysis 2 - Comparing BiasLR among CTL, V400 and V600 groups

Generalized Linear Model

Model Info

Info	Value	Comment
Model Type	Linear	Classical Regression/ANOVA
Call	glm	biasLR ~ 1 + ratGroup + session + ratGroup:session
Link function	Identity	Coefficients in the same scale of y
Distribution	Gaussian	Normal distribution of residual
R-squared	0.1849	Proportion of reduction of error
AIC	-190.0250	Less is better
BIC	-131.3610	Less is better
Deviance	2.3214	Less is better
Residual DF	144	
Chi-squared/DF	0.0161	Overdispersion indicator
Converged	yes	Whether the estimation found a solution

[3]

Model Results

Loglikelihood ratio tests

	X^2	df	p
ratGroup	13.63	2	0.001
session	8.55	5	0.128
ratGroup ✻ session	10.67	10	0.384

Parameter Estimates

					95% Exp(B) Confidence Interval			
Names	Effect	Estimate	SE	exp(B)	Lower	Upper	z	p
(Intercept)	(Intercept)	0.1677	0.0113	1.183	1.157	1.209	14.814	< .001
ratGroup1	V400 - CTL	0.1058	0.0314	1.112	1.045	1.182	3.372	< .001
ratGroup2	V600 - CTL	0.0272	0.0266	1.028	0.975	1.082	1.024	0.308
session1	2 - 1	-0.0708	0.0392	0.932	0.863	1.006	-1.805	0.073
session2	3 - 1	-0.0932	0.0392	0.911	0.844	0.984	-2.377	0.019
session3	4 - 1	-0.0726	0.0392	0.930	0.861	1.004	-1.851	0.066
session4	5 - 1	-0.1022	0.0392	0.903	0.836	0.975	-2.607	0.010
session5	6 - 1	-0.0560	0.0392	0.945	0.876	1.021	-1.429	0.155
ratGroup1 ✻ session1	V400 - CTL ✻ 2 - 1	0.2883	0.1087	1.334	1.078	1.651	2.652	0.009
ratGroup2 ✻ session1	V600 - CTL ✻ 2 - 1	0.1894	0.0920	1.208	1.009	1.447	2.059	0.041
ratGroup1 ✻ session2	V400 - CTL ✻ 3 - 1	0.2317	0.1087	1.261	1.019	1.560	2.131	0.035

ratGroup2 ✻ session2	V600 - CTL ✻ 3 - 1	0.2087	0.0920	1.232	1.029	1.476	2.269	0.025
ratGroup1 ✻ session3	V400 - CTL ✻ 4 - 1	0.2167	0.1087	1.242	1.004	1.537	1.993	0.048
ratGroup2 ✻ session3	V600 - CTL ✻ 4 - 1	0.1656	0.0920	1.180	0.985	1.413	1.800	0.074
ratGroup1 ✻ session4	V400 - CTL ✻ 5 - 1	0.1733	0.1087	1.189	0.961	1.472	1.594	0.113
ratGroup2 ✻ session4	V600 - CTL ✻ 5 - 1	0.0900	0.0920	1.094	0.914	1.310	0.978	0.330
ratGroup1 ✻ session5	V400 - CTL ✻ 6 - 1	0.1650	0.1087	1.179	0.953	1.460	1.518	0.131
ratGroup2 ✻ session5	V600 - CTL ✻ 6 - 1	0.0869	0.0920	1.091	0.911	1.306	0.944	0.347

Estimated Marginal Means

ratGroup

			95% Confidence Interval	
ratGroup	**Mean**	**SE**	**Lower**	**Upper**
CTL	0.123	0.0232	0.0775	0.169
V400	0.229	0.0212	0.1873	0.271
V600	0.151	0.0130	0.1249	0.176

Note. Estimated means are estimated averaging across interacting variables session

			95% Confidence Interval	
session	**Mean**	**SE**	**Lower**	**Upper**
1	0.233	0.0277	0.1787	0.288
2	0.163	0.0277	0.1079	0.218
3	0.140	0.0277	0.0855	0.195
4	0.161	0.0277	0.1061	0.216
5	0.131	0.0277	0.0764	0.186
6	0.177	0.0277	0.1226	0.232

Note. Estimated means are estimated averaging across interacting variables

ratGroup:session

				95% Confidence Interval	
ratGroup	**session**	**Mean**	**SE**	**Lower**	**Upper**
CTL	1	0.2900	0.0568	0.1778	0.402
V400	1	0.2167	0.0518	0.1142	0.319
V600	1	0.1938	0.0317	0.1310	0.256
CTL	2	0.0600	0.0568	-0.0522	0.172

V400	2	0.2750	0.0518	0.1725	0.377
V600	2	0.1531	0.0317	0.0904	0.216
CTL	3	0.0500	0.0568	-0.0622	0.162
V400	3	0.2083	0.0518	0.1059	0.311
V600	3	0.1625	0.0317	0.0998	0.225
CTL	4	0.0900	0.0568	-0.0222	0.202
V400	4	0.2333	0.0518	0.1309	0.336
V600	4	0.1594	0.0317	0.0966	0.222
CTL	5	0.1000	0.0568	-0.0122	0.212
V400	5	0.2000	0.0518	0.0975	0.302
V600	5	0.0937	0.0317	0.0310	0.156
CTL	6	0.1500	0.0568	0.0378	0.262
V400	6	0.2417	0.0518	0.1392	0.344
V600	6	0.1406	0.0317	0.0779	0.203

Plots

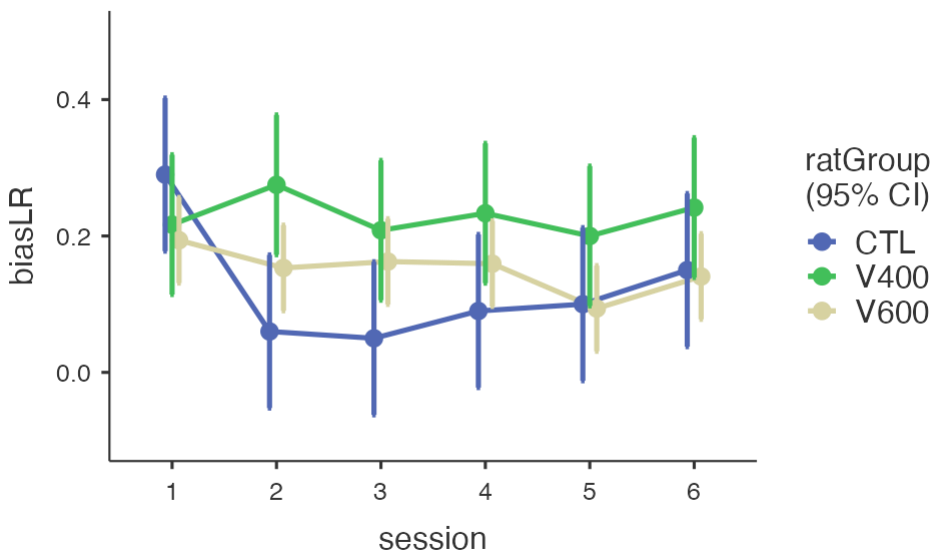

References

[1] The jamovi project (2022). *jamovi*. (Version 2.3) [Computer Software]. Retrieved from https://www.jamovi.org.

[2] R Core Team (2021). *R: A Language and environment for statistical computing*. (Version 4.1) [Computer software]. Retrieved from https://cran.r-project.org. (R packages retrieved from MRAN snapshot 2022-01-01).

[3] Gallucci, M. (2019). *GAMLj: General analyses for linear models*. [jamovi module]. Retrieved from https://gamlj.github.io/.